Materials Research Bulletin 72 (2015) 160–167

Contents lists available at ScienceDirect

Materials Research Bulletin

journal homepage: www.elsevier.com/locate/matresbu

Ferroelectric and piezoelectric responses of (110) and (001)-oriented epitaxial $Pb(Zr_{0.52}Ti_{0.48})O_3$ thin films on all-oxide layers buffered silicon

Hien Thu Vu[a], Minh Duc Nguyen[a,b,c,*], Evert Houwman[b], Muhammad Boota[b], Matthijn Dekkers[c], Hung Ngoc Vu[a], Guus Rijnders[b]

[a] International Training Institute for Materials Science (ITIMS), Hanoi University of Science and Technology, No.1 Dai Co Viet Road, Hanoi 10000, Viet Nam
[b] Inorganic Materials Science (IMS), MESA + Institute for Nanotechnology, University of Twente, P.O. Box 217, 7500 AE Enschede, The Netherlands
[c] SolMateS B.V., Drienerlolaan 5, Building 6, 7522 NB Enschede, The Netherlands

ARTICLE INFO

Article history:
Received 12 April 2015
Received in revised form 17 June 2015
Accepted 28 July 2015
Available online 30 July 2015

Keywords:
A. Thin films
B. Epitaxial growth
B. Laser deposition
B. Piezoelectricity
D. Ferroelectricity

ABSTRACT

Epitaxial ferroelectric $Pb(Zr_{0.52}Ti_{0.48})O_3$ (PZT) thin films were fabricated on silicon substrates using pulsed laser deposition. Depending on the buffer layers and perovskite oxide electrodes, epitaxial films with different orientations were grown. (110)-oriented PZT/$SrRuO_3$ (and PZT/$LaNiO_3$) films were obtained on YSZ-buffered Si substrates, while (001)-oriented PZT/$SrRuO_3$ (and PZT/$LaNiO_3$) were fabricated with an extra CeO_2 buffer layer (CeO_2/YSZ/Si). There is no effect of the electrode material on the properties of the films. The initial remnant polarizations in the (001)-oriented films are higher than those of (110)-oriented films, but it increases to the value of the (001) films upon cycling. The longitudinal piezoelectric $d33_{,f}$ coefficients of the (110) films are larger than those of the (001) films, whereas the transverse piezoelectric $d31_{,f}$ coefficients in the (110)-films are less than those in the (001)-oriented films. The difference is ascribed to the lower density (connectivity between grains) of the former films.
© 2015 Elsevier Ltd. All rights reserved.

1. Introduction

Ferroelectric materials have been used for many years in nonvolatile ferroelectric random access memories (FRAM) [1,2], microsensors and microactuators [3–5], as well as high frequency broadband filter applications [6]. This requires the growth of ferroelectric thin films on a (buffered) semiconducting substrate (e.g., silicon), usually with an interposing metal or conducting metal oxide layer as bottom electrode. The commonly used structure on a Si wafer is a layer of thermally oxidized SiO_2, a thin adhesion enhancing titanium (Ti) layer and a platinum (Pt) layer as the common bottom electrode chosen for its chemical stability in an oxidizing environment and maintaining its conductivity under thermal processing [7,8]. In addition, the bulk resistivity of Pt (10 μW cm) at 20 °C is very good. However, platinized Si substrates have some severe disadvantages. Although good films on such substrates are preferentially (001)-oriented, there is always a significant fraction of other orientations present [9–11]. Further there is no in-plane registry of the film with the substrate. Both aspects result in a polycrystalline film with a large number of grain boundaries. This affects in many cases the lifetime and properties negatively. The disadvantage of reduced lifetime and properties due to the Pt electrodes in direct contact with the ferroelectric can often somewhat be remedied by using a thin intermediate conducting oxide layer. Using appropriate conducting oxide buffer layers it is possible to fabricate all-oxide epitaxial layer devices, with much better or nearly perfect in-plane registry and significantly improved lifetime and properties [12,13]. Recently, epitaxial ferroelectric $Pb(Zr,Ti)O_3$ (PZT) thin films, especially with the composition $Pb(Zr_{0.52}Ti_{0.48})O_3$, have attracted considerable attention in device applications because of their often superior properties over polycrystalline thin films [14–16]. Several studies show that the growth of ferroelectric devices in the form of epitaxial thin films can be performed on both single-crystals (such as $SrTiO_3$, $LaAlO_3$ and MgO) and Si substrates with different conducting perovskite layers as the bottom-electrode [1–21]. Among the perovskite materials, $SrRuO_3$ (SRO) and $LaNiO_3$ (LNO) are not only promising candidates for electrode materials in electroceramic-based devices [22–24] due to their good conductivity, but also good candidates for the epitaxial growth of ferroelectric PZT thin films [25,26]. Moreover, these electrodes

* Corresponding author at: International Training Institute for Materials Science (ITIMS), Hanoi University of Science and Technology, No.1 Dai Co Viet Road, Hanoi 10000, Vietnam. Fax: +84 438692963.
E-mail address: minh.nguyen@itims.edu.vn (M.D. Nguyen).

http://dx.doi.org/10.1016/j.materresbull.2015.07.043
0025-5408/© 2015 Elsevier Ltd. All rights reserved.

have also attracted great attention in recent years due to their ability to drastically improve the ferroelectric fatigue properties of the ferroelectric films, as compared to the conventionally used Pt electrodes [27–29].

In MEMS technology, the most common substrate for micromachining is silicon due to its reliable and reproducible mechanical and electrical properties, its widespread use in electronics and relatively low cost and availability [30,31]. PZT thin films, however, cannot be grown directly on Si because lead can diffuse into silicon substrate to form lead silicates at the growth temperature (500–650 °C) of PZT thin films. Therefore buffer layers between the PZT thin film and the silicon substrate, such as yttria-stabilized zirconia (YSZ), CeO_2 and $SrTiO_3$, are needed to prevent the interdiffusion and oxidation reactions in order to grow highly oriented (epitaxial) PZT thin films on the silicon substrates [13,15,32]. Among these buffer-layers, YSZ is widely used because of its high chemical stability and high electrical resistivity. Moreover, the YSZ layer can be grown heteroepitaxially on a silicon substrate using pulsed laser deposition (PLD) by scavenging the native oxide on the surface of the Si substrate [33]. CeO_2 does not possess this unique feature. A $SrTiO_3$ film can be grown epitaxially, directly on silicon with high structural quality by the molecular-beam epitaxy method [19,34–36].

For device applications, the epitaxial growth of ferroelectric thin films on a silicon substrate is considered to be a key technology for fabricating thinner and smaller electronic devices, because their leakage currents are expected to be lower than of polycrystalline films [37–39]. The properties of thin films are not only affected by the film growth technique, but also by the film crystallographic orientation. One expects a difference in the polarization measured in the direction perpendicular to the substrate surface of a (110)-oriented film with that of the (001)-oriented film and consequently also in the ferroelectric and piezoelectric properties. It is therefore necessary to precisely evaluate the effect of the electrode and buffer layer on the orientation of the functional film in order to improve the device performance. The orientation of epitaxial PZT thin films is usually studied separately from the type of buffer layer, since different buffer layers or electrode materials are used to switch the crystal orientation of epitaxial PZT films on silicon. Hou et al. [40] have studied the growth of perovskite compounds such as $Ba(Sr,Ti)O_3$ and $SrRuO_3$ (SRO) oxide electrodes on a (001)YSZ/Si substrate. The epitaxial relationships between YSZ and these perovskite compounds are (110) perovskite ‖ (001) YSZ / Si. In order to change the orientation of PZT thin films from a (110) to a (001) direction, Kondo et al. [37] and Nordseth et al. [41] have used CeO_2 as a second buffer layer to adjust the large lattice mismatch between YSZ and SRO. Growth of high quality epitaxial films of perovskite oxide electrodes (SRO and LNO) on Si(001) substrates is very important for the application of PZT thin films.

In the present work, we have systematically studied the effects of perovskite thin film buffer layer/electrode combinations on the crystalline orientation and electrical properties of 500 nm thick, epitaxial PZT thin films. By using the same growth technique, deposition apparatus and deposition conditions and only change the buffer layer/electrode stacks we expect that the observed differences between films with different growth orientation can be attributed mainly to the difference in film growth orientation and/or electrode material. To our knowledge such a systematic study does not exist in literature, but is essential to exclude possible differences due to variations in deposition technique, procedures and apparatus. However, it is found that another parameter arises that affects the film properties, i.e. a difference in film density, showing up in different grain connectivity between (110) and (001) oriented films. The PZT/electrode films were grown on YSZ/Si(001) and CeO_2/YSZ/Si(001) substrates.

All buffer layers, electrodes and PZT thin films were deposited using pulsed laser deposition (PLD). The crystalline orientation and crystalline quality of PZT thin films were assessed by X-ray θ–2θ and rocking curve measurements. Ferroelectric and piezoelectric properties were characterized using ferroelectric hysteresis loops and scanning laser Doppler vibrometer measurements, respectively. The relationships between film orientation – film growth – piezoelectric (in-plane and out-of-plane) coefficient have been investigated.

2. Experiment

$Pb(Zr_{0.52}Ti_{0.48})O_3$ (PZT) thin films were grown on different oxide electrodes (SRO and LNO) on (001)/CeO_2/(001)YSZ/(001)Si and (001)YSZ/(001)Si substrates with pulsed laser deposition (PLD), using a KrF excimer laser source (Lambda Physik, 248 nm wavelength) at a fluence of 3.5 J/cm^2 and 10 Hz repetition rate. The deposition temperature and oxygen pressure were fixed at 800 °C and 0.02 mbar O_2 during YSZ and CeO_2 deposition, and 600 °C and 0.13 mbar O_2 during SRO and LNO deposition. The thicknesses of YSZ, CeO_2, SRO and LNO layers were 50, 50, 75 and 75 nm, respectively. The resistivity of the thin-film bottom electrodes was measured using a standard four-point probe method from 0 to 200 °C. The SRO or LNO top electrodes have the same nominal thicknesses and were deposited under the same conditions. The 500 nm PZT thin films were grown at a substrate temperature of 600 °C in a pure oxygen pressure of 0.1 mbar. All layers were deposited successively without breaking the vacuum. After deposition, the stacked film structure was cooled down to room temperature in a 1 bar oxygen atmosphere at a rate of 6 °C/min. The details of the thin film fabrication are shown in Table 1.

Crystallographic properties of the PZT thin films were analyzed by X-ray θ–2θ scans (XRD) and phi- (φ) scans using a Bruker D8 Discover diffractometer.

For electrical measurements, $200 \times 200\ \mu m^2$ capacitors were patterned by a standard photolithography process and structured by argon-beam etching of the top-electrodes and wet-etching (*HF–HCl* solution) of the PZT films. The process for fabricating piezoelectric driven Si cantilevers has been described in a previous paper [16]. Cantilever structures consisting of a piezoelectric stack (SRO/PZT/SRO or LNO/PZT/LNO) on an YSZ and CeO_2/YSZ buffered 10-μm Si-thick supporting layer, were obtained by backside etching of a silicon-on-insulator (SOI) wafer.

The polarization hysteresis (*P-E*) loop measurements were performed with the ferroelectric mode of the aixACCT TF-2000 Analyzer using a triangular *ac*-electric field of ±300 kV/cm at 1 kHz scanning frequency. The polarization-switching cycle

Table 1
Deposition parameters for oxide electrodes and buffer-layers by PLD.

Parameters	Buffer layers		Electrodes		Film
	YSZ	CeO_2	SRO	LNO	PZT
Substrate temperature (°C)	800	800	600	600	600
Oxygen pressure (mbar)	0.02	0.02	0.13	0.13	0.10
Laser fluence (J/cm^2)	2.1	2.5	2.5	2.5	3.5
Laser repetition rate (Hz)	5	5	5	5	10
Thickness (nm)	50	50	75	75	500

Sample	Structures				
S1	Si/YSZ/SRO/PZT/SRO	x		x	
S2	Si/YSZ/LNO/PZT/LNO	x			x
S3	Si/YSZ/CeO_2/SRO/PZT/SRO	x	x	x[a]	
S4	Si/YSZ/CeO_2/LNO/PZT/LNO	x	x		x

[a] The first 20 pulses of SRO (~4 Å) were deposited on CeO_2/YSZ/Si at a higher temperature (800 °C) and in a reducing O_2 environment (<10^{-5} mbar). Afterwards the SRO electrode was then deposited under the given conditions. For the LNO electrode this procedure is not required to obtain (001) growth.

measurements were performed with a bipolar switching pulse of 100 kV/cm pulse height and 5 μs rectangular pulse width at 100 kHz repetition frequency, while the *P-E* loops were measured again at ±300 kV/cm and 1 kHz frequency. The longitudinal piezoelectric coefficient ($d33_{,f}$) of the piezoelectric thin-film capacitors was measured by a Double Beam Laser Interferometer (aixDBLI) method with a driving voltage *ac* signal of ±10 V and 1 kHz. The transverse piezoelectric coefficient $d31_{,f}$ was determined from the tip-displacement of cantilevers, driven by the piezoelectric stack at an *ac*-amplitude of ±3 V (*dc* offset voltage of 3 V) and 8 kHz frequency.

3. Results and discussion

3.1. Thin film characterization

$SrRuO_3$ (SRO) and $LaNiO_3$ (LNO) are metallic perovskite oxides with pseudocubic lattice parameters of 3.93 and 3.84 Å, respectively. The metallic property of the fabricated thin films is demonstrated in the resistivity versus temperature measurements of 75 nm thick SRO and LNO films on YSZ/Si and CeO_2/YSZ/Si substrates as shown in Fig. 1. The room temperature resistivities (25 °C) are 1.87 and 2.23 mΩ cm, for SRO and LNO films deposited on YSZ/Si (resulting in (110) growth), respectively, thus about a factor 5 larger than of bulk metallic samples which are approximately 0.30 and 0.60 mΩ cm. Similar resistivities of 1.76 and 2.17 mΩ cm are obtained for SRO and LNO films on CeO_2/YSZ/Si (resulting in (001)-oriented growth). The strongly increased thin film resistivities are ascribed to enhanced electron scattering at the thin film surfaces and grain boundaries, but there is relatively little effect of the growth orientation and twinning in (110) films compared to (001) films. Further note the slightly larger temperature coefficient of resistance of LNO than that of SRO. These observed resistivities of thin-film electrodes are comparable with previously [42,43], and indicate that the SRO and LNO layers in this study can be a good lattice matched metallic electrode for ferroelectric PZT oxide thin films. Finally we mention for reference that Pt thin film electrodes on Si substrates were found to have a room temperature resistivity in the range 0.18–0.21 mΩ cm [44,45], thus a factor 10 lower than the oxide electrode layers.

Fig. 2 shows the X-ray θ–2θ scan patterns of the PZT thin films deposited on SRO and LNO buffered YSZ/Si and CeO_2/YSZ/Si substrates, respectively. Only preferentially (110)-oriented PZT film growth is observed for the film on SRO/YSZ/Si, while predominantly (110) and a small fraction of (001) PZT growth is observed on LNO/YSZ/Si (see Fig. 2(a) and (c)). On CeO_2/YSZ/Si substrates only (001)-PZT growth is present for both SRO and LNO electrodes (Fig. 2(b) and (d)). This demonstrates that by introducing an extra buffer layer (CeO_2) in the deposition process, the orientation of the PZT thin films can be switched from predominantly (110) to (001).

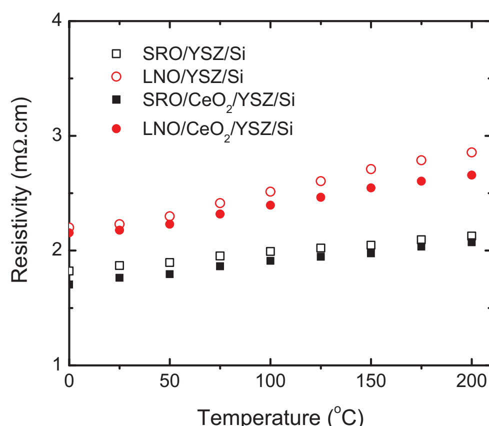

Fig. 1. Temperature dependence of the resistivity of 75 nm thick SRO and LNO thin-film electrodes grown on YSZ/Si and CeO_2/YSZ/Si substrates using PLD.

The full-width at half maximum (FWHM) values of the rocking curves of the PZT(110) peaks are 1.42 and 1.83° for (110)-oriented PZT films on SRO and LNO buffered YSZ/Si, while significantly lower FWHM values of 0.96 and 1.14° of the PZT(002) peaks are observed for the (001)-oriented PZT films on SRO and LNO buffered CeO_2/YSZ/Si. The width of the rocking curves is a measure of the range over which the lattice structure in the different grains tilts with respect to the film normal [14], and is therefore an indication of the homogeneity of the film Fig. 3.

In order to determine the epitaxial relationship between the bottom electrodes and the Si substrate, φ-scan measurements were performed as shown in Fig. 4. Since the lattice parameters of the PZT films almost match those of the bottom electrode materials the crystallographic growth orientation continues that of the underlying electrode.

The in-plane epitaxial relationship between the (001)-oriented buffer-layers (YSZ and CeO_2) and the Si(001) substrates was indicated in a previous paper [13]. The rotation angle φ of the {202} reflection peaks of the CeO_2 and YSZ layers coincide with those of Si. This indicates that a cube-on-cube epitaxial orientation relationship with the Si substrate is obtained for both CeO_2 and YSZ layers, described by (001)YSZ‖(001)Si and (001)CeO_2‖(001)YSZ‖(001)Si. Fig. 4(a) shows the in-plane φ-scan measurements of the (110)-oriented PZT thin films grown on SRO and LNO buffered (001)YSZ/Si. Four identical sets of peaks of PZT{0 0 2} reflections are positioned around the reflections corresponding to Si{2 0 2}. However, instead of a single peak at the Si{2 0 2} position, the intensity is divided over two peaks rotated +10° and −10° with respect to the Si reflection. Since two PZT{0 0 2} peaks are expected in a perfect crystal, this means that twin domains exist in the (110)-oriented thin films [13]. The in-plane φ-scan measurements of the (001)-oriented PZT thin films grown on SRO and LNO buffered (001)CeO_2/YSZ/Si are shown in Fig. 4(b). A 45° shift of the PZT{101} reflections compared to the Si{202} reflections with a fourfold rotational symmetry is found, proving that the unit cells of PZT films are rotated in-plane over 45° with respect to that of the CeO_2/YSZ/Si substrates. Schematic diagrams of the epitaxial relationship between PZT films, perovskite electrodes, YSZ-CeO_2 (fluorite) and silicon (diamond) structures were given in ref. [14].

Fig. 5 shows high resolution scanning electron microscope (HRSEM) images of cross sections of the (110)- and (001)-oriented PZT thin films. The surface of the (001)-oriented films is very smooth reflecting the smooth (001)-oriented surface of the SRO (or LNO)/CeO_2/YSZ/Si. The cross section shows a very dense structure without the clear columnar growth structure observed in the case of the (110)-oriented films. The surfaces of the latter film stacks reflect the columnar structure of the underlying layers starting at the SRO/YSZ (or LNO/YSZ) interface. Secondly in the (110)-oriented films the columnar structure is slightly open for thickness larger than that of an initial growth layer of about 50 nm. The separation of the columns is estimated from these images to be of the order of 7–15 nm and often extends up to the top of the film, although the columns also regularly reconnect. There is no obvious difference in grain connectivity and film density between the (110)-films on SRO or LNO.

Fig. 6 shows the polarization hysteresis loops measured at the initial stage and after 10^{10} switching cycles of PZT thin films on SRO and LNO electrodes buffered, YSZ/Si and CeO_2/YSZ/Si substrates, respectively. Table 2 lists the characteristic ferroelectric and piezoelectric parameters of these films. The saturation polarizations (determined from the crossing of the high-field tangent with the polarization axis) are independent of the type of

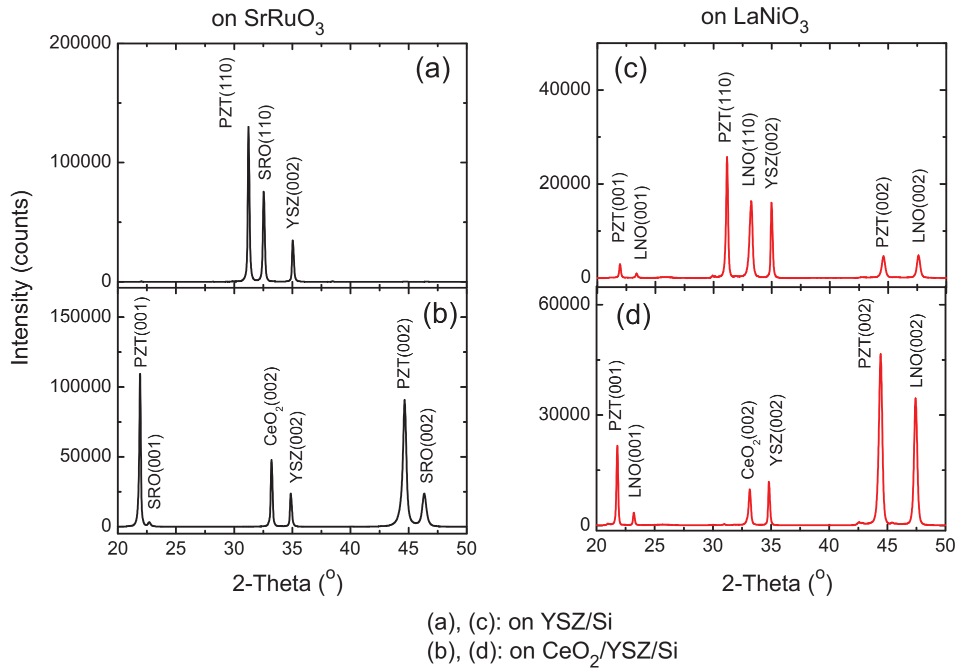

Fig. 2. X-ray θ–2θ scans of PZT films grown on (a,c) YSZ/Si and (b,d) CeO_2/YSZ/Si, with SRO and LNO layers as the bottom electrodes.

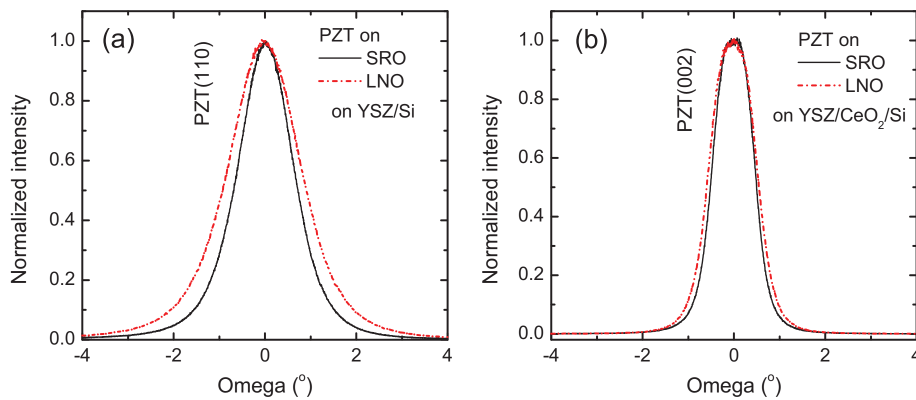

Fig. 3. X-ray rocking curves of (a) PZT(110) peaks of the (110)-oriented PZT films grown on SRO and LNO buffered YSZ/Si; (b) PZT(002) peaks of the (001)-oriented PZT films grown on SRO and LNO buffered CeO_2/YSZ/Si.

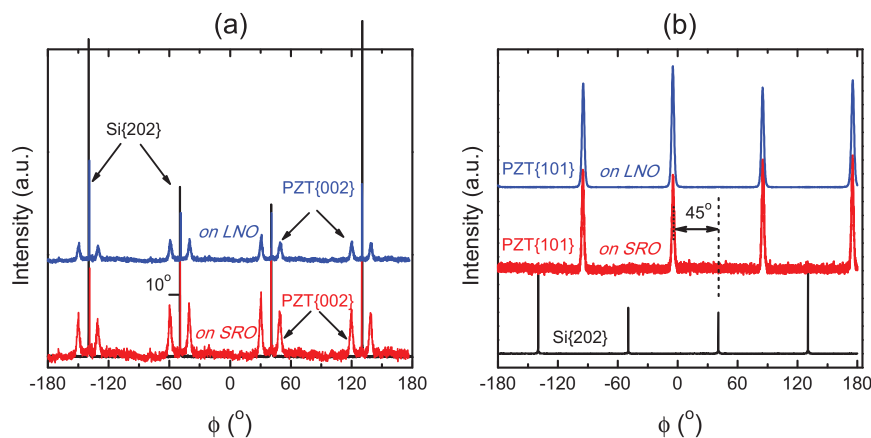

Fig. 4. X-ray φ-scan patterns of (a) PZT{002} reflection of the PZT(110) thin films grown on SRO and LNO electrodes buffered YSZ/Si and (b) PZT{101} reflection of the PZT(001) thin films grown on SRO and LNO electrodes buffered CeO_2/YSZ/Si.

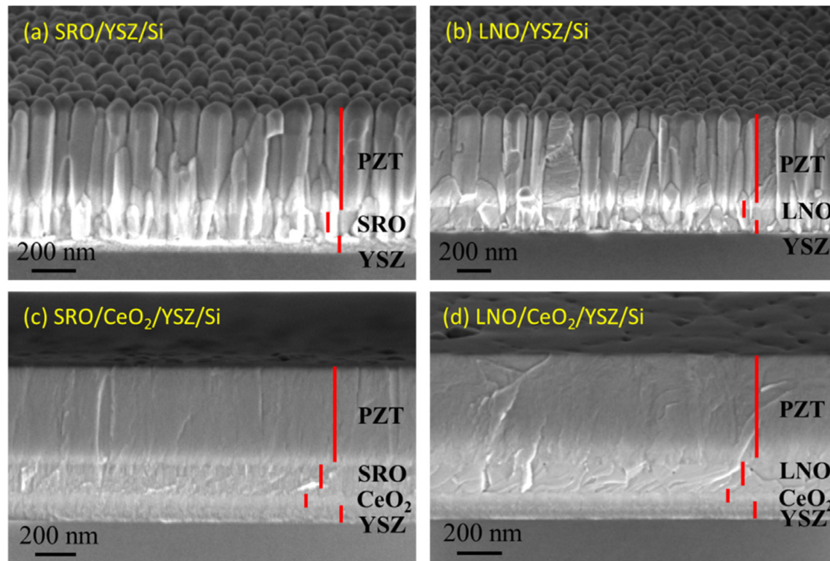

Fig. 5. Cross-sectional HRSEM micrographs of (110)-oriented PZT films on SRO and LNO buffered (a,b) YSZ/Si, respectively, and (c,d) (001)-oriented PZT films on SRO and LNO buffered CeO_2/YSZ/Si.

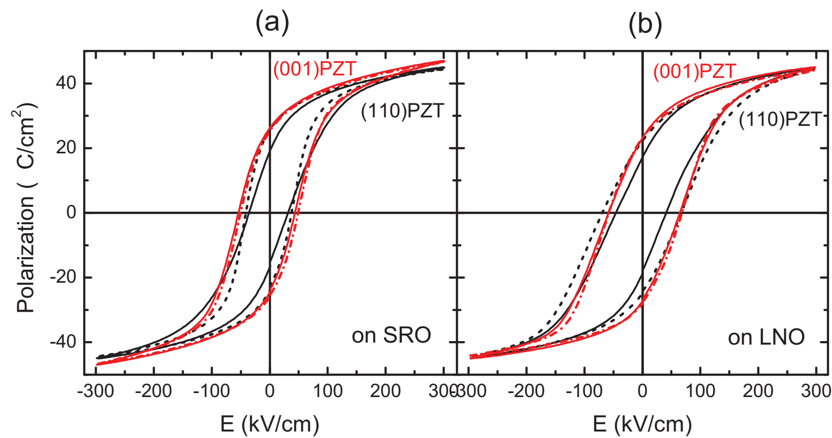

Fig. 6. Initial (dashed) and 10^{10} times cycled (solid) ferroelectric hysteresis loops of (110)- and (001)-oriented PZT films grown on (a) SRO and (b) LNO, buffered YSZ/Si (in black) and CeO_2/YSZ/Si (in red), respectively.

Table 2
Measured properties of PZT thin films on different electrodes buffered YSZ/Si and CeO_2/YSZ/Si substrates.

Sample	Electrode	PZT film orientation	FWHM$_{(peak)}$ (°)	P_r (μC/cm^2)		P_s (μC/cm^2)		$d33_{,f}$ (pm/V) after 10^{10} cycles	$-d31_{,f}$ (pm/V) after 10^{10} cycles
				Initial	10^{10}	Initial	10^{10}		
on YSZ/Si									
S1	SRO	(110)	$1.42_{(110)}$	17.2	24.3	36.2	36.0	110	75
S2	LNO	(110)	$1.83_{(110)}$	17.7	23.6	33.7	34.0	108	72
on CeO_2/YSZ/Si									
S3	SRO	(001)	$0.96_{(002)}$	25.2	25.5	36.6	36.2	80	104
S4	LNO	(001)	$1.14_{(002)}$	25.1	25.3	34.8	34.6	84	98

electrodes and the growth orientation of PZT films. They are also not affected by the cycling. Fig. 7 shows the change in remnant polarization with cycling. The (110)-oriented PZT/SRO and PZT/LNO films in Fig. 7(a) shows an improvement of remnant polarization P_r ($P_r = [P_{r+} - P_{r-}]/2$, where P_{r+} and P_{r-} are the remnant polarization of the positive and negative branches, respectively, of the *P-E* loop) values from 17.2 to 24.3 and from 17.7 to 23.6 μC/cm^2. Previously the improvement of ferroelectric properties with increasing crystalline quality of the PZT film was explained in terms of decreased screening by charged grain boundaries, by removing or compensating these charges with cycling [14]. This also explains the increased squareness of the (110) *P-E* loops with cycling: increase of the remnant polarization and decrease of the relative dielectric constants. Fig. 7(b) gives the results of the fatigue

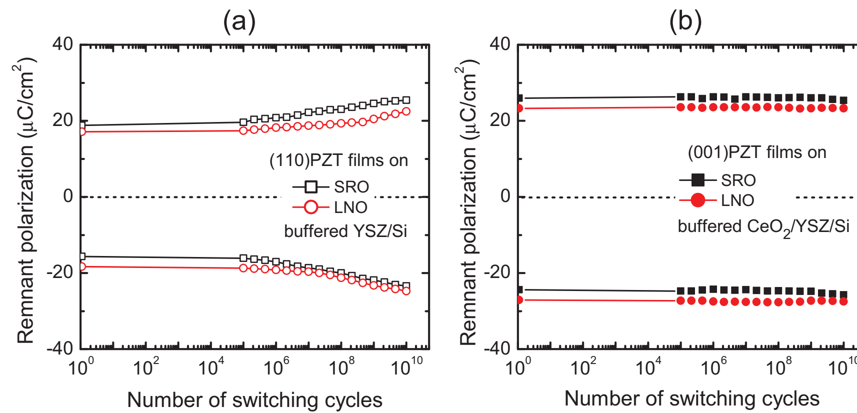

Fig. 7. Remnant polarization as a function of cumulative switching cycles of (a) (110)-oriented PZT/SRO and PZT/LNO films buffered YSZ/Si and (b) (001)-oriented PZT/SRO and PZT/LNO films buffered CeO_2/YSZ/Si.

test on the (001)-oriented PZT films. It shows that these films are very stable. Both (110) and (001) PZT thin films with oxide electrodes show no degradation of *P*r on cycling till 10^{10} cycles. At this cycling number there is no sign of the onset of fatigue yet. This is in marked contrast to PZT/Pt devices, which already degrade after 10^6 cycles [46], and is also a significant improvement over PZT/LNO/Pt/Si devices that degrade after 10^9 cycles [20]. Hence the (CeO_2/)YSZ buffer layer signifies a major improvement with respect to the (LNO/)Pt buffer layer. The difference in cycling behavior between our (001) and (110) films is ascribed to differences in the crystalline structure. Grain boundaries do exist in the (0 0 1) oriented film but these grains are well connected, creating a dense film and oriented coherently in-plane. This in contrast with the (1 1 0) oriented film where the in-plane coherence of the grains is poor and they are much less connected [31]. The grain boundaries between the twinned structural domains in (110) oriented film are formed by defective (likely somewhat charged) crystal faces and cause therefore in the initial stage of cycling some of the polarization in the (110)-film to be screened. These screening charges are assumed to be gradually removed to the film/electrode interface or compensated by opposite charges under cycling, the screened polarization is 'freed' and the remnant polarization reaches the value of the (001)-films. In the case of the (001) films hardly any grain boundaries are present and the screening is negligible from the beginning. We note that oxide electrodes allow easy exchange of oxygen through the film and specifically also out/into the grain boundaries, thus reducing localized charge in the film. Such electrodes also reduce the accumulation of oxygen vacancies near the film-electrode interfaces. Thus oxide electrodes therefore are observed to reduce the suppression of domain switching and interface layer formation and consequently lead to improvement in the fatigue resistance of the ferroelectric capacitors [23,47].

In Fig. 8(a) the dependences of the measured large-signal strain *S* (or out-of-plane displacement Δz) of the (1 1 0)- and (0 0 1)-oriented PZT thin films are shown for the various devices and in Fig. 8(b) the average large signal piezoelectric coefficient $d33_{,f}$, determined as $d33_{,f} = [z(10\,V) - z(0\,V)]/10\,V$, before and after 10^{10} switching cycles. Again it is observed that large signal strain and piezoelectric coefficient are independent of the electrode used, but these parameters do depend on the film orientation. The (110) oriented films have about 25% larger $d33_{,f}$. Although the difference might be ascribed to the different growth orientations, we expect that an important reason is the different density of the film, as will be discussed below. Further experiments with films with different densities are needed to resolve in more detail the connection between growth orientation, grain connectivity and ferroelectric/piezoelectric properties. No change of the piezoelectric parameter is observed after long term cycling. Kim et al. reported on $SrTiO_3$-buffered Si with SRO base electrode and PZT thickness in the range 40 nm–6 μm [48]. The (001)-oriented PZT and SRO were deposited by off-axis rf-magnetron sputtering. A strong thickness dependence of the polarization, peaking at about 2 μm thickness at about 40 μC/cm², significantly larger than the values found in this work. However the polarization value at 500 nm thickness is the same as found here. Also very high piezoelectric coefficient values up to $d33_{,f} = 330$ pm/V for the thickest films were measured. This may be related to the measurement method (piezoresponse force microscopy) used and the cracking of the film at higher thicknesses.

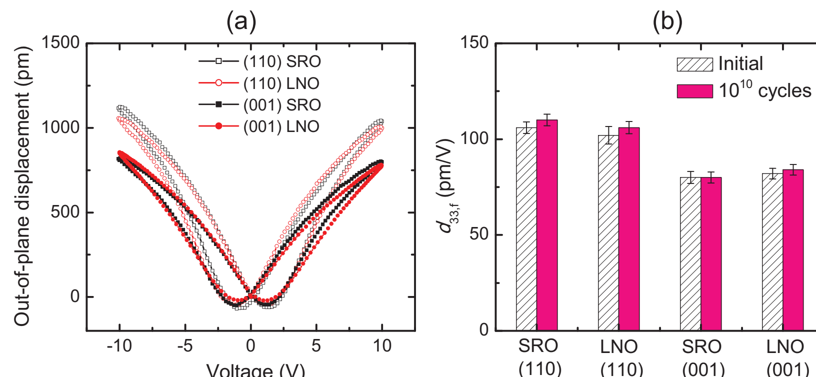

Fig. 8. (a) Piezoelectric large-signal strain S curves (out-of-plane displacement) at the initial stage and (b) Longitudinal piezoelectric coefficient $d33_{,f}$ at the initial stage and after 10^{10} cycles, of PZT thin-film capacitors grown on SRO and LNO buffered YSZ/Si and CeO_2/YSZ/Si.

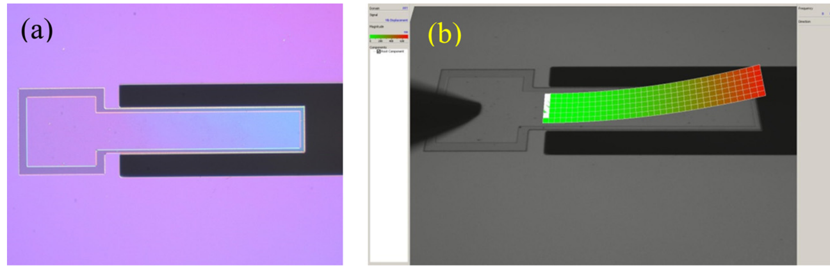

Fig. 9. (a) Microscope image and (b) 3-dimensional scanning actuator image of the upward displacement, of a PZT/Si-beam cantilever (400 × 100 × 10 "long × width × thick" in μm).

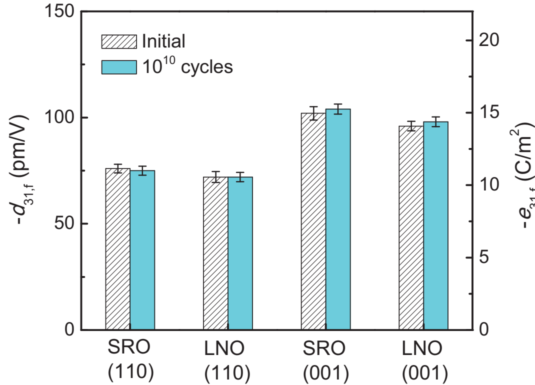

Fig. 10. Transverse piezoelectric coefficients ($d31_{,f}$ and $e31_{,f}$) of 400×100×10 (long×width×thick) in μm Si-beam cantilevers based on PZT films grown on SRO and LNO electrodes buffered YSZ/Si and CeO_2/YSZ/Si, at the initial stage and after 10^{10} cycles.

Further the film composition $Pb(Zr_{0.45}Ti_{0.55})O_3$ was changed from that of the target $Pb(Zr_{0.52}Ti_{0.48})O_3$.

3.2. Cantilever characterization

A microscope image (top-view) of a 400 × 100 (length×width in μm) cantilever with a 500 nm-thick PZT actuator thin film on top of a 10 μm-thick Si beam is shown in Fig. 9(a). Fig. 9(b) shows a typical three-dimensional piezoelectric displacement response of the cantilever measured by scanning laser Doppler vibrometer (LDV, Polytec's MSA-400 Micro System Analyzer) at an *ac*-voltage of ±3 V (*dc* offset voltage of 3 V) and 8 kHz frequency (off-resonant frequency).

The transverse piezoelectric coefficients ($d31_{,f}$) of the PZT thin films were evaluated from the tip-displacements from the following equation [49]:

$$d_{31,f} = \frac{\sum_{i}^{n} E_i A_i (t_i^2/12 + z_i^2)}{E_p Z_p w_p} \frac{2\delta_T}{L^2 V_{ac}} \quad (1)$$

where z_i is the center of each layer (layer i), measured from the neutral axis of the cantilever [50], and $A_i = w_i t_i$ is the cross-sectional area of layer i. E_i,w_i and t_i are theYoung's modulus, the width and the thickness of the layer, respectively; n is the total number of layers and L the cantilever length. The subscript "p" denotes the piezoelectric film. Material parameters used are given in Ref. [16]. The piezoelectric parameter $e31_{,f}$ is calculated as $e31_{,f} = d31_{,f}/(s11_{,p} + s12_{,p})$, where $s11_{,p}$ and $s12_{,p}$ are the elastic compliances of the piezoelectric film. The obtained values are given in Fig. 10. It is seen that there is no dependence on cycling and electrode material, but a large dependence on growth orientation. The obtained $d31_{,f}$ values of the (001)-films are about 30% less than the bulk value (−156 pm/V) for this composition [51]. The difference is ascribed to the clamping of the film, reducing the lateral contraction. Consequently also $d33_{,f}$ of the (001) is expected to be diminished, because the film cannot extend in the field direction as much as in bulk due to the clamping. The much lower measured $d31_{,f}$ values of the (110)-oriented film as compared to the (001)-films are believed to have a different cause. The very open columnar structure makes a large fraction of the film ineffective in contracting the film as a whole. The columns contract in width with applied field, but since they are not connected over most of the film thickness the film itself is much less contracted, giving rise to much less tip deflection and therefore an apparent lower $d31_{,f}$ of the film. Thus to achieve larger film transverse piezoelectric coefficients one should strive to produce denser films.

4. Conclusions

The crystallographic growth orientation of PLD-derived PZT thin films depends on the choice of the silicon substrates/buffers layers, but is independent of the chosen perovskite oxide electrodes used in this paper (LNO or SRO). Epitaxial (001)-oriented PZT films were obtained on silicon substrates with an YSZ/ CeO_2 bilayer buffer as seed layer for the electrode growth, while epitaxial (110)-oriented PZT films grow on silicon substrates with a single YSZ buffer layer.

1) PZT thin films on oxide-electrodes (SRO or LNO) can be switched completely from (110) to (001) orientation when an additional buffer-layer CeO_2 is used on YSZ/Si.
2) (001)-oriented PZT films exhibit a higher initial polarization as compared to the (110)-oriented films. This is ascribed to partial screening of the polarization due to a large amount of charged grain boundaries in the latter films. With progressing cycling the charges are neutralized and the remnant polarization reaches the value of the (001) films.
3) The ferroelectric properties of the (001)-oriented PZT thin films are stable on cycling while those of the (110)-films improve. The piezoelectric properties of all films do not change on cycling, irrespective of buffer layer and electrode layer.
4) (110)-oriented PZT films show a larger $d33_{,f}$ but smaller $d31_{,f}$ than the (001)-oriented films. These differences are tentatively ascribed to the different density (connectivity between grains) between these films. The last finding indicates that the piezoelectric properties can be changed by changing the density of the PZT. This is important for choosing the proper film growth orientation for specific applications which require either a large in-plane or out-of-plane piezoelectric displacement.

Further experimental work is required to establish the relation between film growth orientation, film density/grain connectivity and film properties.

Acknowledgements

This work is financially supported by the Vietnamese MOET Science and Technology Research Program under Grant number B2014-01-62, and by the NanoNextNL, a micro and nanotechnology consortium of the Government of the Netherlands and 130 partners.

References

[1] J.F. Scott, C.A. Paz de Araujo, Science 246 (1989) 1400–1405.
[2] S.-T. Han, Y. Zhou, V.A.L. Roy, Adv. Mater. 25 (2013) 5425–5449.
[3] Y. Qiu, J.V. Gigliotti, M. Wallace, F. Griggio, C. Demore, S. Cochran, S. Trolier-McKinstry, Sensors 15 (2015) 8020–8041.
[4] G. Marrazza, Biosensors 4 (2014) 301–317.
[5] J.N. Blake, R. Mutharasan, Analyst 139 (2014) 1112–1120.
[6] H. Yagubizade, M. Darvishi, Y.-Y. Chen, M.D. Nguyen, J.M. Dekkers, R.J. Wiegerink, M.C. Elwenspoek, N.R. Tas, Appl. Phys. Lett. 102 (2013) 063509.
[7] A. Kumar, M.R. Alam, A. Mangiaracina, M. Shamsuzzoha, J. Electron. Mater. 26 (1997) 1331–1334.
[8] Y. Fujisaki, K. Kushida-Abdelghafar, Y. Shimamoto, H. Miki, J. Appl. Phys. 82 (1997) 341–344.
[9] J.-H. Park, S.H. Yoon, D. Shen, S.-Y. Choe, Y.S. Yoon, M. Park, D.-J. Kim, J. Mater. Sci: Mater. Electron. 20 (2009) 366–373.
[10] N. Setter, D. Damjanovic, L. Eng, G. Fox, S. Gevorgian, S. Hong, A. Kingon, H. Kohlstedt, N.Y. Park, G.B. Stephenson, I. Stolitchnov, A.K. Taganstev, D.V. Taylor, T. Yamada, S. Streiffer, J. Appl. Phys. 100 (2006) 051606.
[11] S. Trolier-McKinstry, P. Muralt, J. Electroceram. 12 (2004) 7–17.
[12] E.M. Alkoy, S. Alkoy, K. Uchiyama, T. Shiosaki, Jpn. J. Appl. Phys. 45 (2006) 5110–5116.
[13] M. Dekkers, M.D. Nguyen, R. Steenwelle, P.M. te Riele, D.H.A. Blank, G. Rijnders, Appl. Phys. Lett. 95 (2009) 012902.
[14] H. Funakubo, M. Dekkers, A. Sambri, S. Gariglio, I. Shklyarevskiy, G. Rijnders, MRS Bulletin 37 (2012) 1030–1038.
[15] D. Isarakorn, A. Sambri, P. Janphuang, D. Briand, S. Gariglio, J.-M. Triscone, F. Guy, J.W. Reiner, C.H. Ahn, N.F. de Rooij, J. Micromech. Microeng. 20 (2010) 055008.
[16] M.D. Nguyen, M. Dekkers, H.N. Vu, G. Rijnders, Sens. Act. A 199 (2013) 98–105.
[17] J. Schwarzkopf, R. Fornari, Prog. Cryst. Growth Charact. Mater. 52 (2006) 159–212.
[18] I. Vrejoiu, M. Alexe, D. Hesse, U. Gösele, Adv. Funct. Mater. 18 (2008) 3892–3906.
[19] S.-H. Baek, C.-B. Eom, Acta Materialia 61 (2013) 2734–2750.
[20] C.R. Cho, Mater. Sci. Eng. B 64 (1999) 113–117.
[21] E.P. Houwman, M.D. Nguyen, M. Dekkers, G. Rijnders, Sci. Technol. Adv. Mater. 14 (2013) 045006.
[22] C.B. Eom, R.J. Cava, R.M. Fleming, J.M. Phillips, R.B. vanDover, J.H. Marshall, J.W. P. Hsu, J.J. Krajewski, W.F. Peck, Jr, Science 258 (1992) 1766–1769.
[23] C.B. Eom, R.B. vanDover, J.M. Phillips, D.J. Werder, J.H. Marshall, C.H. Chen, R.J. Cava, R.M. Fleming, D.K. Fork, Appl. Phys. Lett. 63 (1993) 2570–2572.
[24] C.L. Chen, Y. Cao, Z.J. Huang, Q.D. Jiang, Z. Zhang, Y.Y. Sun, W.N. Kang, L.M. Dezaneti, W.K. Chu, C.W. Chu, Appl. Phys. Lett. 71 (1997) 1047–1049.
[25] A.P. Chen, F. Khatkhatay, W. Zhang, C. Jacob, L. Jiao, H. Wang, J. Appl. Phys. 114 (2013) 124101.
[26] T. Yu, Y.-F. Chen, Z.-G. Liu, S.-B. Xiong, L. Sun, X.-Y. Chen, L.-J. Shi, N.-B. Ming, Appl. Phys. Lett. 69 (1996) 2092–2094.
[27] A.L. Kholkin, E.L. Colla, A.K. Tagantsev, D.V. Taylor, N. Setter, Appl. Phys. Lett. 68 (1996) 2577–2579.
[28] M.D. Nguyen, H. Nazeer, K. Karakaya, S.V. Pham, R. Steenwelle, M. Dekkers, L. Abelmann, D.H.A. Blank, G. Rijnders, J. Micromech. Microeng. 20 (2010) 085022.
[29] B.G. Chae, Y.S. Yang, S.H. Lee, M.S. Jang, S.J. Lee, S.H. Kim, W.S. Baek, S.C. Kwon, Thin Solid Films 410 (2002) 107–113.
[30] K. Petersen, Proc. IEEE 70 (1982) 420–457.
[31] J. Du, W.H. Ko, D.J. Young, Sen. Act. A 112 (2004) 116–121.
[32] A. Lin, X. Hong, V. Wood, A.A. Verevkin, C.H. Ahn, R.A. McKee, F.J. Walker, E.D. Specht, Appl. Phys. Lett. 78 (2001) 2034–2036.
[33] S.J. Wang, C.K. Ong, L.P. You, S.Y. Xu, Semicond. Sci. Technol. 15 (2000) 836–839.
[34] J.Q. He, C.L. Jia, V. Vaithyanathan, D.G. Schlom, J. Schubert, A. Gerber, H.H. Kohlstedt, R.H. Wang, J. Appl. Phys. 97 (2005) 104921.
[35] X.Y. Zhou, J. Miao, J.Y. Dai, H.L.W. Chan, C.L. Choy, Y. Wang, Q. Li, Appl. Phys. Lett. 90 (2007) 012902.
[36] M. Spreitzer, R. Egoavil, J. Verbeeck, D.H.A. Blank, G. Rijnders, J. Mater. Chem. C 1 (2013) 5216–5222.
[37] M. Kondo, K. Maruyama, K. Kurihara, FUJITSU Sci. Tech. J. 38 (2002) 46–53.
[38] S. Yamauchi, M. Yoshimaru, Jpn. J. Appl. Phys. 35 (1996) 1553–1556.
[39] C.J. Kim, D.S. Yoon, J.S. Lee, C.G. Choi, W.J. Lee, K. No, J. Appl. Phys. 76 (1994) 7478–7482.
[40] S.Y. Hou, J. Kwo, R.K. Watts, J.-Y. Cheng, D.K. Fork, Appl. Phys. Lett. 67 (1995) 1387–1389.
[41] Ø. Nordseth, T. Tybell, J.K. Grepstad, Thin Solid Films 517 (2009) 2623–2626.
[42] S.-G. Yoon, Epitaxial $SrRuO_3$ thin films deposited on SrO buffered-Si(001) substrates for ferroelectric $Pb(Zr_{0.2}Ti_{0.8})O_3$ thin films, in: I. Coondoo (Ed.), Ferroelectrics, InTech Europe, Croatia, 2010, pp. 89–98.
[43] H. Kim, J.-H. Kim, W.K. Choo, J. Korean Phys. Soc. 43 (2003) 847–849.
[44] U. Schmid, H. Seidel, Thin Solid Films 516 (2008) 898–906.
[45] J.S. Agustsson, U.B. Arnalds, A.S. Ingason, K.B. Gylfason, K. Johnsen, S. Olafsson, J.T. Gudmundsson, Appl. Surf. Sci. 254 (2008) 7356–7360.
[46] M.D. Nguyen, E. Houwman, M. Dekkers, H.N. Vu, G. Rijnders, Sci. Adv. Mater. 6 (2014) 243–251.
[47] D.-H. Do, P.G. Evans, E.D. Isaacs, D.M. Kim1, C.B. Eom, E.M. Dufresne, Nat. Mater. 3 (2004) 365–369.
[48] D.M. Kim, C.B. Eom, V. Nagarajan, J. Ouyang, R. Ramesh, V. Vaithyanathan, D.G. Schlom, Appl. Phys. Lett. 88 (2006) 142904.
[49] M. Dekkers, H. Boschker, M. van Zalk, M. Nguyen, H. Nazeer, E. Houwman, G. Rijnders, J. Micromech. Microeng. 23 (2013) 025008.
[50] D. Campolo, Energy efficient driving of piezoelectric actuators for the micromechanical flying insect, Ph.D. thesis, Nanyang Technological University, Singapore, 2001.
[51] M.J. Haun, S.J. Furman, L.E. Cross, Ferroelectrics 99 (1989) .